

Impeding Macrophage Entry into Hypoxic Tumor Areas by Sema3A/Nrp1 Signaling Blockade Inhibits Angiogenesis and Restores Antitumor Immunity

Andrea Casazza,^{1,2} Damya Laoui,^{3,4} Mathias Wenes,^{1,2} Sabrina Rizzolio,⁵ Nicklas Bassani,^{1,2} Marco Mambretti,^{1,2} Sofie Deschoemaeker,^{1,2} Jo A. Van Ginderachter,^{3,4} Luca Tamagnone,⁵ and Massimiliano Mazzone^{1,2,*}

¹Laboratory of Molecular Oncology and Angiogenesis, Vesalius Research Center, VIB, 3000 Leuven, Belgium

²Laboratory of Molecular Oncology and Angiogenesis, Department of Oncology, Vesalius Research Center, KU Leuven, 3000 Leuven, Belgium

³Laboratory of Myeloid Cell Immunology, VIB, 1050 Brussels, Belgium

⁴Laboratory of Cellular and Molecular Immunology, Department of Molecular and Cellular Interactions, Vrije Universiteit Brussel, 1050 Brussels, Belgium

⁵Institute for Cancer Research at Candiolo, Department of Oncology, University of Torino, 10060 Candiolo, Torino, Italy

*Correspondence: massimiliano.mazzone@vib-kuleuven.be

<http://dx.doi.org/10.1016/j.ccr.2013.11.007>

SUMMARY

Recruitment of tumor-associated macrophages (TAMs) into avascular areas sustains tumor progression; however, the underlying guidance mechanisms are unknown. Here, we report that hypoxia-induced Semaphorin 3A (Sema3A) acts as an attractant for TAMs by triggering vascular endothelial growth factor receptor 1 phosphorylation through the associated holoreceptor, composed of Neuropilin-1 (Nrp1) and PlexinA1/PlexinA4. Importantly, whereas Nrp1 levels are downregulated in the hypoxic environment, Sema3A continues to regulate TAMs in an Nrp1-independent manner by eliciting PlexinA1/PlexinA4-mediated stop signals, which retain them inside the hypoxic niche. Consistently, gene deletion of Nrp1 in macrophages favors TAMs' entrapment in normoxic tumor regions, which abates their pro-angiogenic and immunosuppressive functions, hence inhibiting tumor growth and metastasis. This study shows that TAMs' heterogeneity depends on their localization, which is tightly controlled by Sema3A/Nrp1 signaling.

INTRODUCTION

Inflammatory / immune responses mostly involve the recruitment of circulating monocytes to specific locations, such as intratumoral areas, bacterial entry sites, arthritic joints, infarcted lesions, or atherosclerotic plaques (Eltzschig and Carmeliet, 2011). In particular, macrophages infiltrating the tumor, named tumor-associated macrophages (TAMs), represent the most abundant stromal component of many cancer types and the presence of extensive TAM infiltration, often but not always, correlates with poor prognosis in a variety of human carcinomas

(De Palma and Lewis, 2013; Johansson et al., 2008). This is because TAMs entail protumoral functions, but they were also reported to be antitumoral (Biswas and Mantovani, 2010; Cousens et al., 2013; Johansson et al., 2008). Such opposed TAM phenotypes occupy distinct niches in the tumor, thus raising the question whether this may reflect "education" of the macrophages by specific signals in the tumor microenvironment and/or whether TAM subsets might derive from distinct macrophage precursors (Murdoch and Lewis, 2005).

Neuropilin-1 (Nrp1) was originally identified as a receptor for class-3 semaphorins controlling neuronal guidance and axonal

Significance

TAM infiltration of human cancers was reported to correlate with opposed prognoses because TAMs can be either pro- or antitumoral. Here, we show that TAMs' localization into hypoxic tumor areas is controlled by a Sema3A/Neuropilin-1 signaling axis, leading to PlexinA1/PlexinA4-dependent VEGFR1 activation. Once in the hypoxic environment, TAMs are arrested because of Nrp1-independent PlexinA1/PlexinA4-mediated stop signals. We found that confining TAMs inside normoxic regions by blunting the Sema3A/Neuropilin-1 pathway restores anti-tumor immunity and abates angiogenesis, overall inhibiting tumor growth and metastasis. These results underscore the predictive value of macrophage association with tumor hypoxia and suggest alternative approaches to hijack TAMs against cancer by modulating their localization within the tumor, and thus their phenotype.

growth (Gu et al., 2003; Kolodkin et al., 1997). Besides playing a decisive role in the developing nervous system, Nrp1 is expressed in a variety of non-neural cells and can modulate multiple physiological and pathological processes (Gerhardt et al., 2004; Gu et al., 2003; Hayashi et al., 2012; Liang et al., 2007; Soker et al., 1998). Preclinical data suggest that blockade of Nrp1 suppresses tumor growth by inhibiting angiogenesis or by impairing survival and proliferation in a variety of cancer cell types (Hong et al., 2007; Liang et al., 2007; Pan et al., 2007).

Nrp1 is also widely expressed in lymphoid and myeloid cells (Bruder et al., 2004; Fantin et al., 2010; Pucci et al., 2009). In vitro and in vivo studies have identified a regulatory role of this molecule in immune responses, cell proliferation, chemotaxis, and cytokine production of T cells and dendritic cells (DCs) (Catalano, 2010; Catalano et al., 2006; Delgoffe et al., 2013; Hansen et al., 2012; Takamatsu et al., 2010; Tordjman et al., 2002). Other studies, also from our laboratory, have described Nrp1 as a marker of pro-angiogenic and pro-arteriogenic macrophages in physiological and pathological conditions (Fantin et al., 2010; Pucci et al., 2009; Rolny et al., 2011; Takeda et al., 2011). Nevertheless, the functional relevance of this molecule in macrophages is not known.

By using genetic tools and several tumor mouse models, we study how Nrp1 controls TAMs' entry into hypoxic regions in response to its ligand Semaphorin 3A.

RESULTS

Loss of Nrp1 in Macrophages Inhibits Tumor Progression

By intercrossing Nrp1 floxed mice with LysM-Cre mice, we generated LysM-Cre;Nrp1^{L/L} mice where Nrp1 expression is reduced by 92% in TAMs and 81% in their monocyte precursors, but less than 60% in tumor-associated neutrophils (TANs) or DCs (Figure S1A available online). Compared to littermate controls (LysM-Cre;Nrp1^{+/+}; wild type [WT] in short), LysM-Cre;Nrp1^{L/L} mice were normal and had similar blood counts (Table S1 and Fantin et al., 2013); however, the implantation of subcutaneous Lewis lung carcinomas (LLC) resulted in 60% smaller tumors and 55% fewer pulmonary metastases (Figures 1A–1C). Tumor apoptosis was increased in LysM-Cre;Nrp1^{L/L} mice (Figure S1B) but proliferation was unchanged (Figure S1C). Tumor vessel area, density and branching points, together with vessel perfusion, were strongly decreased in LysM-Cre;Nrp1^{L/L} mice (Figures 1D–1I).

To achieve specific deletion of Nrp1 in macrophages, but not in other myeloid cells (Figure S1D and Qian et al., 2011), we intercrossed Nrp1 floxed mice with the tamoxifen-inducible iCSF1R-Cre line, thus generating iCSF1R-Cre;Nrp1^{L/L} mice. Acute deletion of Nrp1 shortly before LLC tumor injection, abated tumor growth, metastasis, and vessel formation to a similar extent as in LysM-Cre;Nrp1^{L/L} mice (Figures 1J–1L; Figures S1E and S1F). Thus, Nrp1 loss in TAMs inhibits cancer progression and angiogenesis.

Loss of Nrp1 in TAMs Prevents Their Entry into Hypoxic Niches

To quantify tumor infiltration of myeloid cells in WT and LysM-Cre;Nrp1^{L/L} mice, we stained tumor sections for the pan-myeloid

marker CD11b. Tumors in LysM-Cre;Nrp1^{L/L} mice were infiltrated with almost twice more myeloid cells than in the controls (Figures S1G–S1I). Among all the CD11b⁺ myeloid cells, only TAMs, but not TANs or DCs, were more abundant in LysM-Cre;Nrp1^{L/L} versus WT mice (Figures 1M–1O; Figure S1J). Increased TAM density was not associated to a difference in the frequency of total circulating monocytes or monocyte subsets (“inflammatory” CD115⁺Ly6C^{high} versus “resident” CD115⁺Ly6C^{low} monocytes), TAM proliferation, or TAM apoptosis (Figures S1J–S1M). Moreover, in a model of acute skin inflammation, macrophage infiltration was equally induced in both genotypes, suggesting that Nrp1 deletion did not affect monocyte recruitment or their differentiation into macrophages (Figure S1N).

We reasoned that the rise of TAMs in LysM-Cre;Nrp1^{L/L} mice was due to increased tumor hypoxia (Eltzschig and Carmeliet, 2011; Murdoch and Lewis, 2005), possibly resulting from reduced tumor perfusion. Indeed, the hypoxic tumor area was 2.2-times higher in LysM-Cre;Nrp1^{L/L} than in WT mice (Figures 1P and 1R). Conversely, at early stages (when tumor volume and weight were comparable in both genotypes), the amount of hypoxic areas as well as TAMs did not change (Figures S1O–S1R), suggesting that increased TAM infiltration in LysM-Cre;Nrp1^{L/L} mice was secondary to tumor progression and augmented hypoxia. Consistently, hypoxia-induced monocyte attractants such as Ccl2, Csf1, and Csf2 were comparable in both genotypes at short term, but they were higher in LysM-Cre;Nrp1^{L/L} mice at the end stage, the time point when TAMs' frequency increases in these mice (Figures S1S–S1U). Strikingly, in LysM-Cre;Nrp1^{L/L} mice, TAMs were found mostly in normoxic (PIMO-negative) regions, and their accumulation inside hypoxic areas was instead greatly prevented both at early (Figure S1V) and end stage (Figures 1S–1U). In LysM-Cre;Nrp1^{L/L} mice as well, total hypoxic area and total density of TAMs in end-stage tumors were augmented but TAM accumulation within the hypoxic regions was reduced (Figures 1V–1X). Apoptosis and proliferation of WT and Nrp1-knockout (KO) TAMs or bone marrow-derived macrophages (BMDMs), cultured in either normoxia (21% O₂) or hypoxia (1% O₂) for 36 hr, did not differ (not shown). Altogether, these data indicate that Nrp1 is not directly involved in macrophage recruitment to the tumor but might rather be involved in TAM entry into hypoxic niches.

TAM Redistribution by Nrp1 Loss Hinders Orthotopic and Spontaneous Tumors

Because the microenvironment strongly influences tumor responses (Blouw et al., 2003), we evaluated how Nrp1 loss in TAMs affected the progression of several orthotopic tumors. First, we injected LLC cancer cells directly in the lungs. Sixteen days after injection, 47% of WT mice and only 8% of LysM-Cre;Nrp1^{L/L} mice died (Figure 2A). Of all the survivors, whole lung weight in WT mice was 63% higher than in LysM-Cre;Nrp1^{L/L} mice and tumor expansion in WT mice completely destroyed the structure of the pulmonary parenchyma whereas this was better preserved in LysM-Cre;Nrp1^{L/L} mice (Figures 2B–2D).

Because pancreatic cancers expressing higher VEGF or Sema3A levels have worse prognosis (Biankin et al., 2012; Müller et al., 2007; Niedergethmann et al., 2002), we injected Panc02

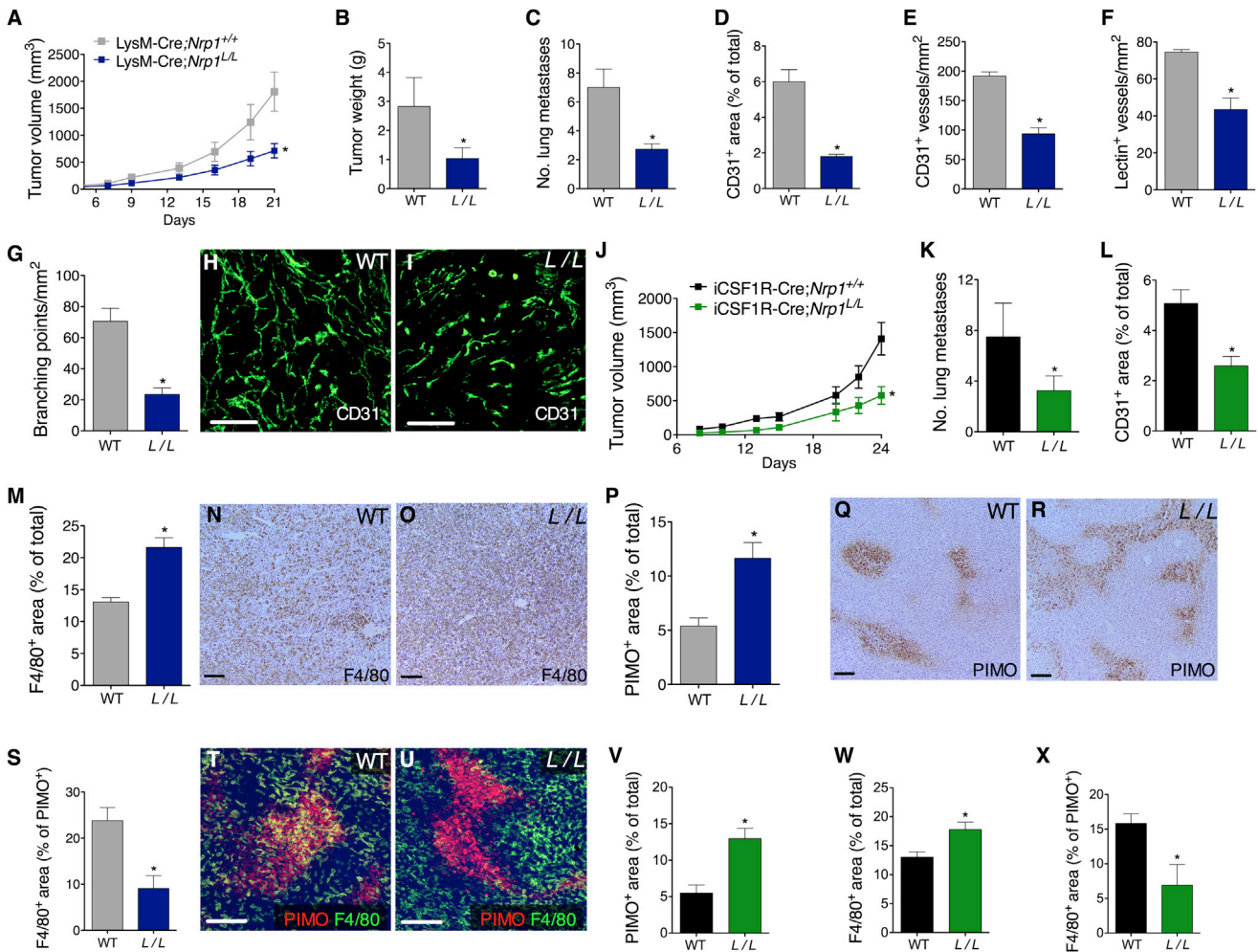


Figure 1. Loss of *Nrp1* in TAMs Inhibits Their Entry into Hypoxic Niches

(A–C) Subcutaneous LLC tumor growth (A), weight (B), and lung metastases (C) in mice with myeloid cell-specific deletion of *Nrp1* (LysM-Cre;*Nrp1*^{L/L}; L/L in short) and controls (LysM-Cre;*Nrp1*^{+/+}; WT in short).

(D–F) Tumor vessel area (D), density (E), and perfusion (F) in WT and LysM-Cre;*Nrp1*^{L/L} (L/L) mice.

(G–I) Vessel branching quantification (G) and micrographs (H and I) on CD31-stained LLC tumor thick-sections.

(J–L) Subcutaneous LLC tumor growth (J), lung metastases (K), and tumor vessel density (L) in mice with macrophage-specific deletion of *Nrp1* (iCSF1R-Cre;*Nrp1*^{L/L}; L/L in short) and controls (iCSF1R-Cre;*Nrp1*^{+/+}; WT in short).

(M–O) F4/80 quantification (M) and micrographs (N and O) showing TAM infiltration of end-stage subcutaneous LLC tumors in WT and LysM-Cre;*Nrp1*^{L/L} (L/L) mice.

(P–R) Quantification (P) and micrographs of pimonidazole (PIMO)-stained LLC tumor sections in WT and LysM-Cre;*Nrp1*^{L/L} (L/L) mice (Q and R).

(S–U) Morphometric quantification (S) and micrographs (T, U) of LLC tumor sections stained for F4/80 and PIMO, showing TAM infiltration of hypoxic tumor regions in WT and LysM-Cre;*Nrp1*^{L/L} (L/L) mice.

(V–X) Tumor hypoxia (V) and TAM infiltration of the overall tumor sections (W) or of hypoxic tumor regions (X) in WT and iCSF1R-Cre;*Nrp1*^{L/L} (L/L) mice.

All experiments, n = 8. *p < 0.05 versus WT. Scale bars: 100 μm. All graphs show mean ± SEM. See also Figure S1 and Table S1.

pancreatic cancer cells orthotopically in WT and LysM-Cre;*Nrp1*^{L/L} mice. Also in this case, end-stage tumor weight was reduced by 60% in LysM-Cre;*Nrp1*^{L/L} versus WT mice (Figure 2E). The number of metastatic lymph nodes in the mesentery of LysM-Cre;*Nrp1*^{L/L} mice was two times lower than that found in WT mice (Figure 2F).

To prevent inflammation caused by technical procedures (i.e., needle injection), we intercrossed WT and LysM-Cre;*Nrp1*^{L/L} mice with mice expressing the PyMT oncoprotein under the control of the mouse mammary tumor virus promoter (MMTV-PyMT), a mouse model that spontaneously develops multiple metastatic

mammary gland carcinomas (Lin et al., 2003). In this genetic background, tumors reached end stage in 22-week-old control mice. LysM-Cre;*Nrp1*^{L/L} littermates had 50% smaller tumors (Figures 2G–2I). Although the overall tumor incidence did not differ between genotypes, LysM-Cre;*Nrp1*^{L/L} mice displayed more hyperplastic and intraepithelial neoplastic lesions but fewer early and late carcinomas (Figures 2J and 2K). Furthermore, lung metastases in these mice were 80% less than those in controls (Figure 2L).

Similar to what observed in subcutaneous LLC tumors, all these orthotopic models displayed higher tumor hypoxia and

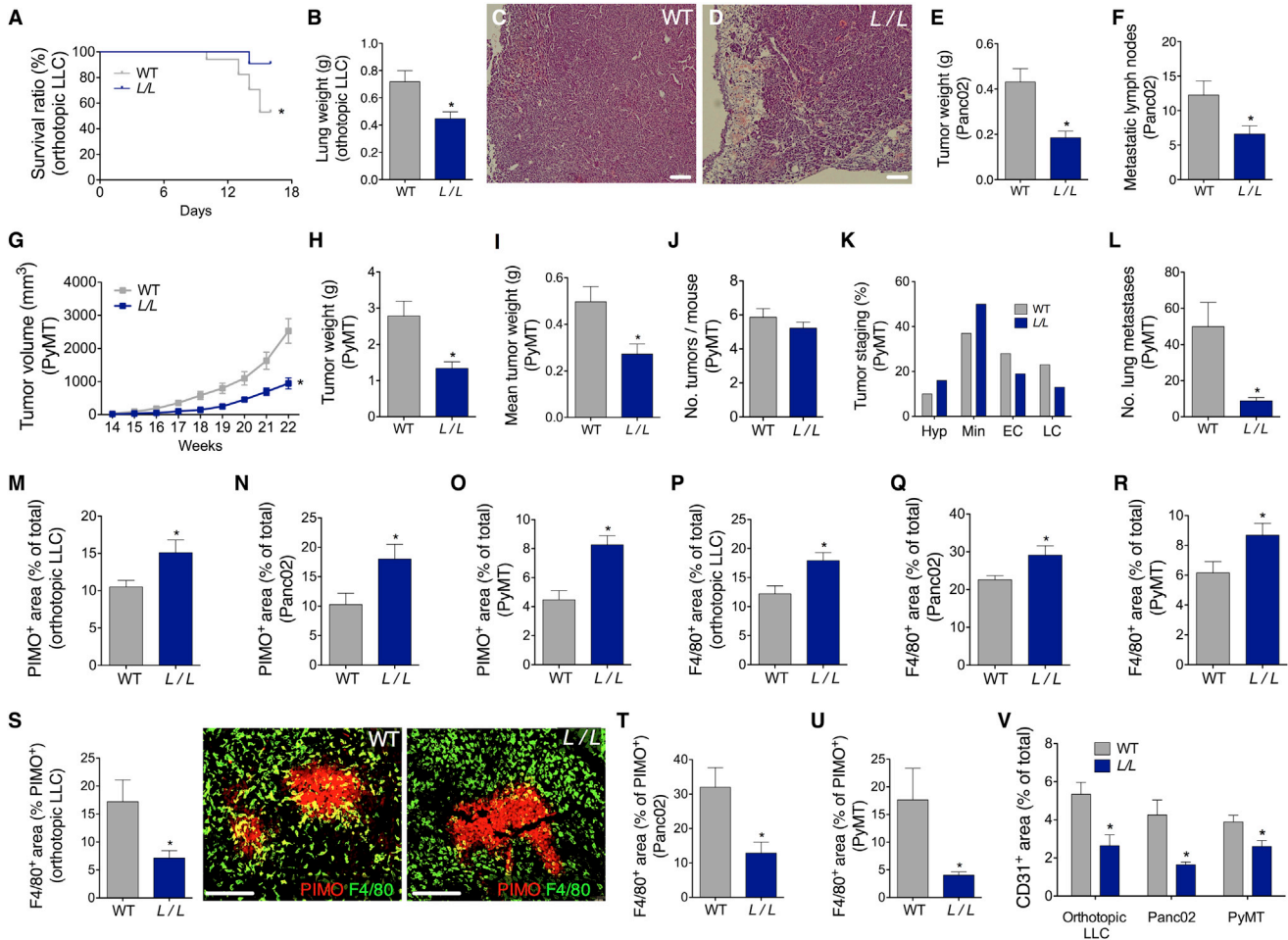


Figure 2. Loss of *Nrp1* in TAMs Abates Orthotopic Tumor Growth and Metastasis

(A–D) Kaplan-Meier at 16 days (n = 11–17; A), lung weight (B), and pulmonary structure by hematoxylin and eosin staining (C and D) in WT and *LysM-Cre;Nrp1^{L/L}* (*L/L*) mice orthotopically implanted with LLC tumors (n = 7).

(E and F) Orthotopic Panc02 tumor weight (E) and number of metastatic mesenteric lymph nodes (F) in WT and *LysM-Cre;Nrp1^{L/L}* (*L/L*) mice. n = 9.

(G–J) Total tumor volume (G), total (H) and mean (I) tumor weight, and tumor incidence (J) in WT and *LysM-Cre;Nrp1^{L/L}* (*L/L*) mice intercrossed with a mouse strain developing spontaneous breast cancer (PyMT). n = 14.

(K) Frequency of hyperplastic (Hyp) or intraepithelial (Min) neoplastic mammary lesions compared to the frequency of early (EC) or late (LC) PyMT mammary carcinomas.

(L) Number of lung metastatic nodules arising from PyMT tumors.

(M–R) Hypoxic PIMO⁺ areas (M–O) and TAM accumulation (P–R) in the indicated tumor model.

(S–U) Quantification and representative images of TAMs in PIMO⁺ regions in the indicated tumor model.

(V) Tumor vessel area in the indicated tumor model.

*p < 0.05 versus WT. Scale bars: 100 μ m. All graphs show mean \pm SEM.

TAM infiltration in *LysM-Cre;Nrp1^{L/L}* than in WT mice (Figures 2M–2R); however, *Nrp1*-KO TAMs failed to enter hypoxic niches (Figures 2S–2U). This phenotype was associated with reduced tumor vascularization (Figure 2V). Altogether, these data show that TAM redistribution by loss of *Nrp1* is accompanied by a slower progression of several orthotopic tumors independently from their tissue of origin.

TAM Redistribution by *Nrp1* Loss Restores Immunity and Reduces Angiogenesis

Because TAMs in *LysM-Cre;Nrp1^{L/L}* mice failed to enter hypoxic tumor regions, we studied the effect on their phenotype.

Compared to WT TAMs, TAMs from *LysM-Cre;Nrp1^{L/L}* mice were less potent in promoting endothelial cell (EC) migration and in inducing the formation of EC capillary networks, either when co-cultured directly with ECs or upon stimulation of ECs with TAM-conditioned media (Figures 3A–3E; Figure S2A–S2D). Furthermore, TAMs from *LysM-Cre;Nrp1^{L/L}* mice released more nitric oxide (NO; Figure 3F), were more cytotoxic against cancer cells (Figure 3G), and displayed reduced T cell suppression (thus increasing T cell proliferation; Figure 3H). Notably, all these functions did not differ between WT and *Nrp1*-KO BMDMs (Figures 3A–3C and 3F–3H; Figures S2A and S2B), suggesting that the different distribution of

TAMs in *LysM-Cre;Nrp1^{L/L}* mice, not *Nrp1* loss per se, strongly affects their phenotype.

The *in vitro* effects of *Nrp1*-KO TAMs on ECs are in agreement with the reduced tumor vessel density/area and vascular complexity observed in *LysM-Cre;Nrp1^{L/L}* mice. Because *Nrp1*-KO TAMs also had a milder T cell immunosuppressive capacity, we analyzed how this translated *in vivo*. The frequency of CD4⁺ T helper cells (Th) in subcutaneous LLC tumors was similar in both genotypes whereas intratumoral CD8⁺ cytotoxic T lymphocytes (CTLs) were 1.6-times more abundant in *LysM-Cre;Nrp1^{L/L}* than in WT mice (Figures 3I–3L). Despite their comparable numbers, CD4⁺ lymphocytes in *LysM-Cre;Nrp1^{L/L}* mice displayed higher expression of antitumoral Th1 markers (Figure 3M). Enhanced CTL recruitment and Th1 T cell skewing, following *Nrp1* loss in myeloid cells, was also observed in PyMT spontaneous breast tumors (Figure 3N). This pronounced Th1/CTL response was associated with an enriched expression of antitumoral M1 genes and decrease of some protumoral M2 markers in TAMs sorted from *LysM-Cre;Nrp1^{L/L}* mice (Figures 3O–3V). However, these genes were equally expressed in cultured WT and *Nrp1*-KO BMDMs, either at baseline (in normoxia or hypoxia) or under forced M1/M2-skewing conditions (Figures S2E–S2L), suggesting that the M1 profile of *Nrp1*-KO TAMs was secondary to microenvironmental changes in the tumor (see below).

When administering anti-CD4 and anti-CD8 antibodies, alone or in combination, depletion of Th cells and/or CTLs in *LysM-Cre;Nrp1^{L/L}* mice mildly (but not significantly) increased growth and weight of subcutaneous LLC tumors compared to tumors treated with an isotype IgG (Figures 4A and 4B). In contrast, depletion of Th cells or CTLs in *LysM-Cre;Nrp1^{L/L}* mice resulted in accelerated LLC tumor growth, reaching comparable sizes as tumors in WT mice (Figures 4A and 4B). Depletion of both CD4⁺ and CD8⁺ T cells had similar effects as depletion of CD8⁺ T cells alone, indicating that CTLs are the main effectors of tumor inhibition in *LysM-Cre;Nrp1^{L/L}* mice (Figures 4A and 4B). The efficiency of intratumoral CD4⁺ cell depletion was almost complete in both WT and *LysM-Cre;Nrp1^{L/L}* mice, and anti-CD8 antibodies did not affect the frequency of Th cells in both genotypes (Figure 4C). Conversely, tumor-infiltrating CTLs were 2.3 times more abundant in *LysM-Cre;Nrp1^{L/L}* versus WT mice, but they were reduced by 40%, 90%, and 96%, respectively, following anti-CD4, anti-CD8, or combined treatment (Figure 4D). Circulating CD4⁺ and CD8⁺ cell numbers did not differ in both WT and *LysM-Cre;Nrp1^{L/L}* mice, and treatment with anti-CD4 and/or anti-CD8 antibodies depleted these cells from the bloodstream almost completely in both genotypes (Figure S3). Reduction of tumor vessel area and density in *LysM-Cre;Nrp1^{L/L}* mice was independent from Th cells and/or CTLs (Figures 4E and 4F). Instead, the excess of M1-like TAMs in *LysM-Cre;Nrp1^{L/L}* mice was abrogated, partly, by Th cell depletion and, completely, by CTL depletion (Figure 4G).

These data demonstrate that inhibition of TAMs' entry into hypoxic niches hinders their angiogenic and immunosuppressive potential while fostering Th1 cells and CTLs, which, in turn, will sustain macrophage cytotoxicity and adaptive anti-tumor immunity.

***Nrp1* Is Transcriptionally Repressed in Hypoxic Macrophages**

Finally, we studied how *Nrp1* could be mechanistically involved in TAM positioning inside the hypoxic regions. First, we determined how oxygen tension affects *Nrp1* expression in macrophages. In BMDMs, *Nrp1* transcripts were reduced by 80% in hypoxia compared to normoxia (Figure 5A). Similarly, freshly isolated hypoxic (PIMO-positive) TAMs expressed 90% less *Nrp1* than the normoxic (PIMO-negative) counterpart (Figure 5B). The efficiency of gene deletion was complete in both normoxic and hypoxic BMDMs or TAMs isolated from *LysM-Cre;Nrp1^{L/L}* mice (Figures 5A and 5B). Also in tumor sections, *Nrp1* was almost undetectable in WT TAMs localized within hypoxic (PIMO-positive) areas; as expected, *Nrp1* staining was always negative in TAMs from *LysM-Cre;Nrp1^{L/L}* mice (Figure 5C). In contrast, the hypoxia-responsive gene *Flt1* (encoding vascular endothelial growth factor receptor 1 [VEGFR1]) was 5-fold induced in hypoxic versus normoxic BMDMs or TAMs, and *Nrp1* deletion did not affect this regulation (Figures 5D and 5E).

We then measured the expression of *Sema3a* and *Vegfa* in hypoxic (PIMO-positive) and normoxic (PIMO-negative) tumor single cell suspensions that contain cancer cells and stromal cells. Both genes were upregulated in the hypoxic fraction of the tumor (Figures 5F and 5G). Consistently, both *Sema3a* and *Vegfa* were induced in LLC cancer cells cultured in hypoxia (1% O₂; Figures 5H and 5I).

When seeking the molecular mechanisms underlying hypoxic repression of *Nrp1* in macrophages, we found that gene deletion of *Hif2a* but not *Hif1a* completely abrogated this downregulation (Figure 5J). In particular, HIF-2 only was entirely responsible for the hypoxic induction of *Ikbkg* and, in good part, of *Ikbkb*, together forming the IKK complex, required for the activation of the canonical NF-κB pathway (Figures 5K and 5L), which can repress *Nrp1* (Hayashi et al., 2012). Indeed, genetic inactivation of this pathway in *Ikbkb*-KO macrophages prevented *Nrp1* downregulation by hypoxia; overexpression of p50/p65 NF-κB subunits in *Hif2a*-KO or *Ikbkb*-KO macrophages restored this transcriptional repression (Figure 5J). These data indicate that hypoxic stabilization of HIF-2 in macrophages unleashes the canonical NF-κB pathway via IKK induction. Consequently, release of active p50/p65 heterodimers blocks *Nrp1* expression.

***Nrp1* Regulation by Hypoxia Defines Macrophage Responses to Sema3A**

Prompted by the above observations, we assessed the chemotactic potential of Sema3A or VEGF on WT and *Nrp1*-KO macrophages, isolated respectively from WT and *LysM-Cre;Nrp1^{L/L}* mice. In the presence of Sema3A, migration of WT BMDMs was doubled whereas *Nrp1*-KO BMDMs did not respond. VEGF₁₆₄ was equally potent but the absence of *Nrp1* decreased this migratory response by only 30%. Thus, *Nrp1* is strictly necessary for macrophage attraction by Sema3A, but not by VEGF₁₆₄. Indeed, VEGF₁₂₀ (which does not bind *Nrp1* effectively; Soker et al., 1998) was as good as VEGF₁₆₄ in attracting both WT and *Nrp1*-KO BMDMs (Figure 6A). In line with the migratory phenotype, Sema3A and VEGF₁₆₄ induced cytoskeleton remodeling and macrophage elongation; however, while the absence of *Nrp1* completely abrogated Sema3A activity, it marginally reduced the response to VEGF₁₆₄ (Figure S4A).

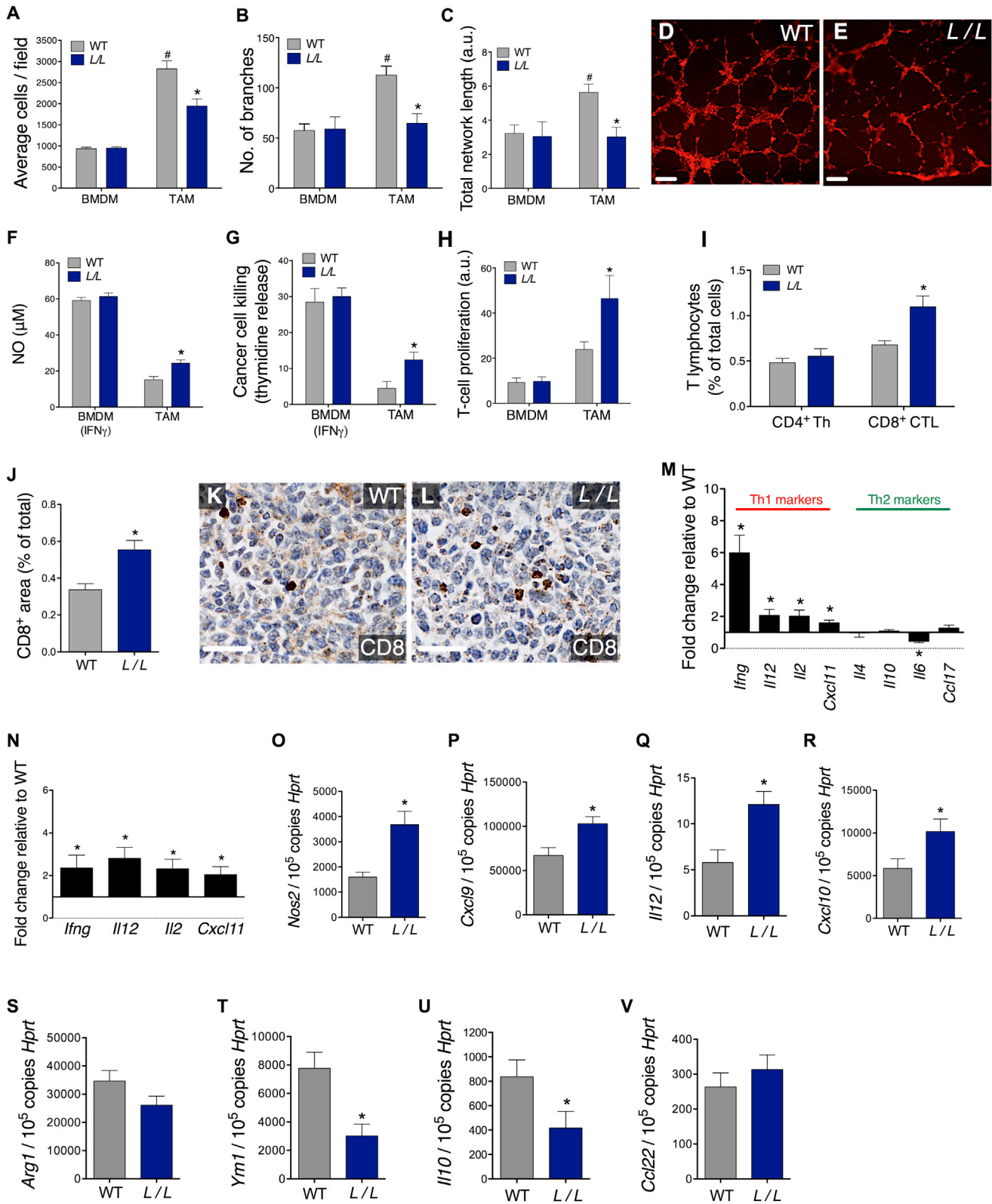


Figure 3. Exclusion of *Nrp1*-KO TAMs from Hypoxic Areas Prevents Their Angiogenic Phenotype and Restores Their Antitumor Features (A–E) Histograms showing HUVEC migration toward BMDMs or TAMs isolated from WT or LysM-Cre;*Nrp1*^{L/L} (*L/L*) mice (A), and HUVEC organization (in red), as measured by their branch number (B) and total network length (C) in co-culture with TAMs (D and E). (F–H) Nitric oxide (NO) release (F), cytotoxicity on thymidine-labeled LLC cancer cells (G), and T cell suppression (H) by BMDMs or TAMs.

(legend continued on next page)

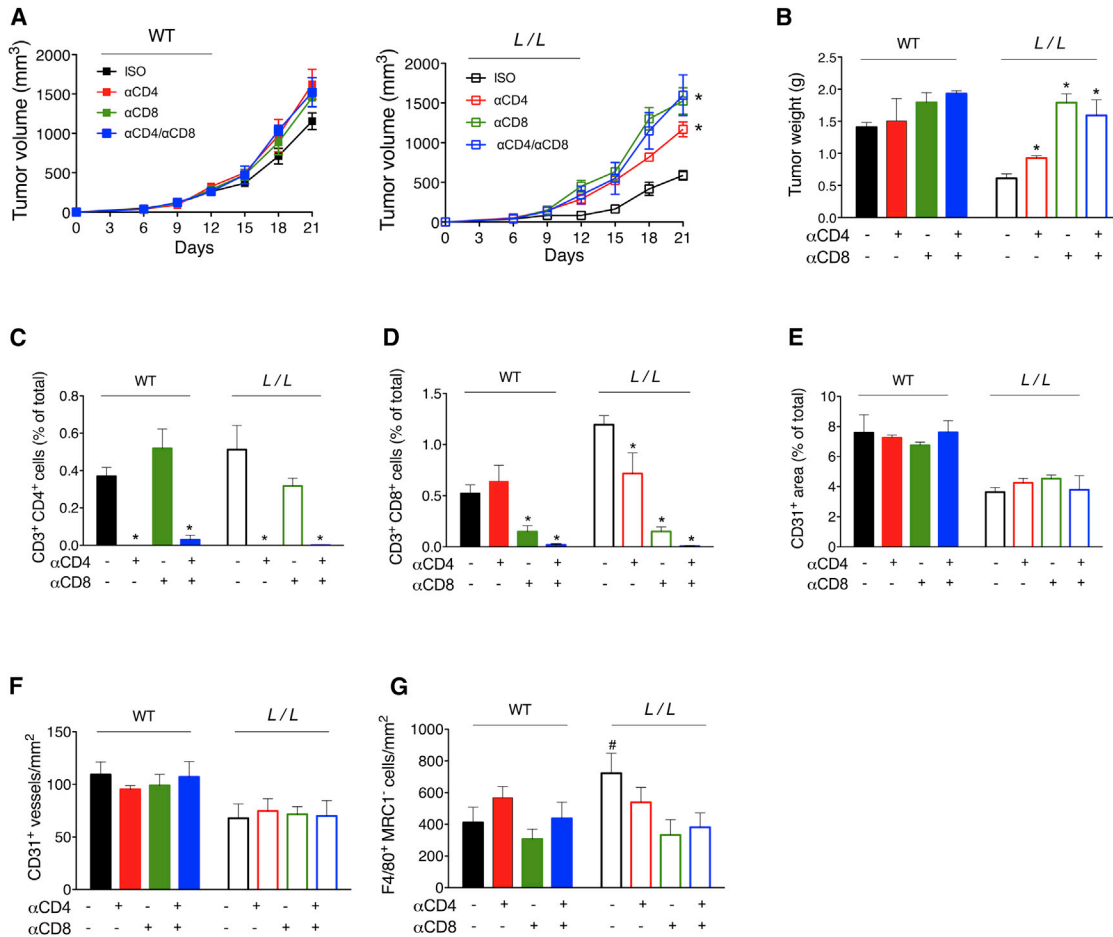


Figure 4. TAM Redistribution by *Nrp1* Loss Favors T Cell-Mediated Antitumor Immunity

(A and B) Subcutaneous LLC tumor growth in WT (A, left) and *LysM-Cre;Nrp1^{L/L}* (*L/L*) mice (A, right), and their end-stage tumor weights (B), following systemic administration of CD4 and CD8 neutralizing antibodies, alone or in combination.

(C and D) Efficiency of Th cell (C) or CTL (D) depletion in the tumors.

(E and F) Quantification of vessel area (E) and vessel density (F) on LLC tumor sections.

(G) Quantification of F4/80⁺MRC1⁺ M1-like TAM infiltration on LLC tumor sections.

All experiments, n = 6–8. *p < 0.05 versus IgG control. All graphs show mean ± SEM. See also Figure S3.

Similar results were obtained *in vivo*, where subcutaneous matrigel plugs containing recombinant *Sema3A*, *VEGF₁₆₄*, or *VEGF₁₂₀* displayed a strong and comparable macrophage infiltration. Loss of *Nrp1* reduced macrophage attraction to *Sema3A* by 50% and to *VEGF₁₆₄* by 20% only, whereas *VEGF₁₂₀* activity did not change (Figure 6B).

Because *Sema3A* and *VEGF₁₆₄* are present together in the tumor and are both induced by hypoxia, we assessed *in vitro* macrophage migration in response to combined *Sema3A* and

VEGF₁₆₄ under either normoxia or hypoxia (1% O₂). Interestingly, in normoxia, this combination did not further increase the migration of WT macrophages compared to either cytokine alone, whereas *Nrp1*-KO macrophages further lost their migratory response to VEGF (Figure 6C). In hypoxia, neither WT nor *Nrp1*-KO macrophages were attracted toward *Sema3A* (consistent with hypoxia-mediated and genetic-driven *Nrp1* loss, respectively); conversely, their response to *VEGF₁₆₄* was even stronger than in normoxia (Figure 6D), likely because of

(I) FACS quantification on single cell LLC tumor suspensions of CD4⁺ Th cells and CD8⁺ cytotoxic T lymphocytes (CTLs).

(J–L) Quantification (J) and micrographs (K and L) of CD8-stained LLC tumor sections.

(M and N) Expression of Th1 (*Ifng*, *Il12*, *Il2*, *Cxcl11*) and Th2 (*Il4*, *Il10*, *Il6*, *Ccl17*) genes in tumor-infiltrating CD4⁺ Th cells sorted from subcutaneous LLC (M) or PyMT tumors (N) in *LysM-Cre;Nrp1^{L/L}* (*L/L*) mice, normalized to the expressions in WT controls.

(O–V) Expression of the M1 markers *Nos2* (O), *Cxcl9* (P), *Il12* (Q), *Cxcl10* (R), and the M2 markers *Arg1* (S), *Ym1*, (T), *Il10* (U), *Ccl22* (V) in TAMs sorted from subcutaneous LLC tumors.

All experiments, n = 6–12. *p < 0.05 versus WT; #p < 0.05 versus BMDMs. Scale bars: 50 μm (D and E) and 25 μm (K and L). All graphs show mean ± SEM. See also Figure S2.

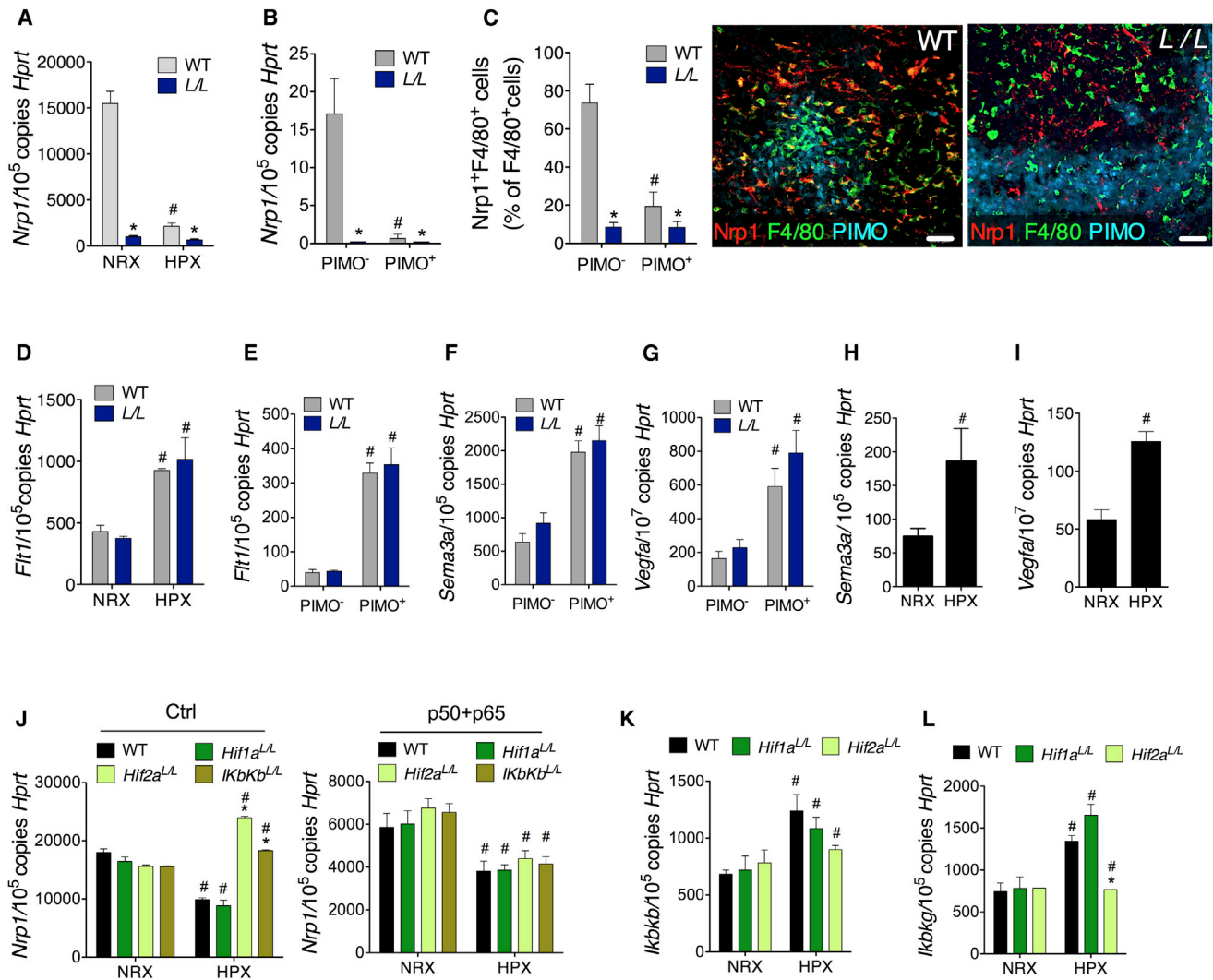


Figure 5. Hypoxic Repression of *Nrp1* in Macrophages Is Mediated by HIF2-Dependent NF-κB Activity

(A) *Nrp1* expression in BMDMs derived from WT and LysM-Cre;*Nrp1*^{L/L} (L/L) mice and cultured in normoxia (21% O₂; NRX) or hypoxia (1% O₂; HPX). (B) *Nrp1* expression in normoxic (PIMO⁻) or hypoxic (PIMO⁺) TAMs (E) directly sorted from WT and LysM-Cre;*Nrp1*^{L/L} (L/L) mice. (C) Quantification and representative micrographs of Nrp1⁺F4/80⁺ TAMs in normoxic (PIMO⁻) or hypoxic (PIMO⁺) tumor areas. (D and E) *Flt1* expression in normoxic (NRX) or hypoxic (HPX) BMDMs (D) and in normoxic (PIMO⁻) or hypoxic (PIMO⁺) TAMs (E). (F and G) *Sema3a* (F) or *Vegfa* (G) induction in hypoxic (PIMO⁺) versus normoxic (PIMO⁻) tumor cell bulks from either WT or LysM-Cre;*Nrp1*^{L/L} (L/L) mice. (H and I) *Sema3a* (H) and *Vegfa* (I) expression in cultured LLC cancer cells. (J) *Nrp1* transcript levels in WT, *Hif1a*-KO (*Hif1a*^{L/L}), *Hif2a*-KO (*Hif2a*^{L/L}), and *Ikbkb*-KO (*Ikbkb*^{L/L}) BMDMs, electroporated with a control (Ctrl) plasmid (on the left) or with two plasmids overexpressing the NF-κB subunits p50 and p65 (on the right), and cultured under normoxic (NRX) or hypoxic (HPX) conditions. (K and L) *Ikbkb* (K) and *Ikbkg* (L) expression in normoxic (NRX) and hypoxic (HPX) WT, *Hif1a*-KO (*Hif1a*^{L/L}), *Hif2a*-KO (*Hif2a*^{L/L}) BMDMs. n = 8 in (A–G) and n = 4 in (H–L). *p < 0.05 versus WT controls; #p < 0.05 versus NRX or PIMO⁻. Scale bars: 100 μm. All graphs show mean ± SEM.

hypoxia-mediated VEGFR1 induction. However, the migration of hypoxic macrophages (either WT or *Nrp1*-KO) was barely induced upon combined stimulation with Sema3A and VEGF₁₆₄ (Figure 6D).

These data suggest a *Nrp1*-independent function of Sema3A antagonizing VEGF-induced attraction and prompted our search for evidence that Sema3A can interact with macrophages even in the absence of *Nrp1*. Cell-binding experiments in situ with alkaline-phosphatase (AP) tagged molecules demonstrated that Sema3A binding is also remarkably present on *Nrp1*-KO cells

(about 50% less than in WT cells), as validated by specific competition by unlabeled Sema3A (Figure 6E). Thus, Sema3A can specifically interact with *Nrp1*-KO macrophages, potentially accounting for the functional activity observed in hypoxic conditions.

The chemokine CCL21 can elicit macrophage egression from tumor hypoxic niches because its levels are much higher in normoxic versus hypoxic cancer cells (Figure S4B). Remarkably, Sema3A significantly reduced the migration toward CCL21 of *Nrp1*-KO or hypoxic WT macrophages, where *Nrp1* is also barely

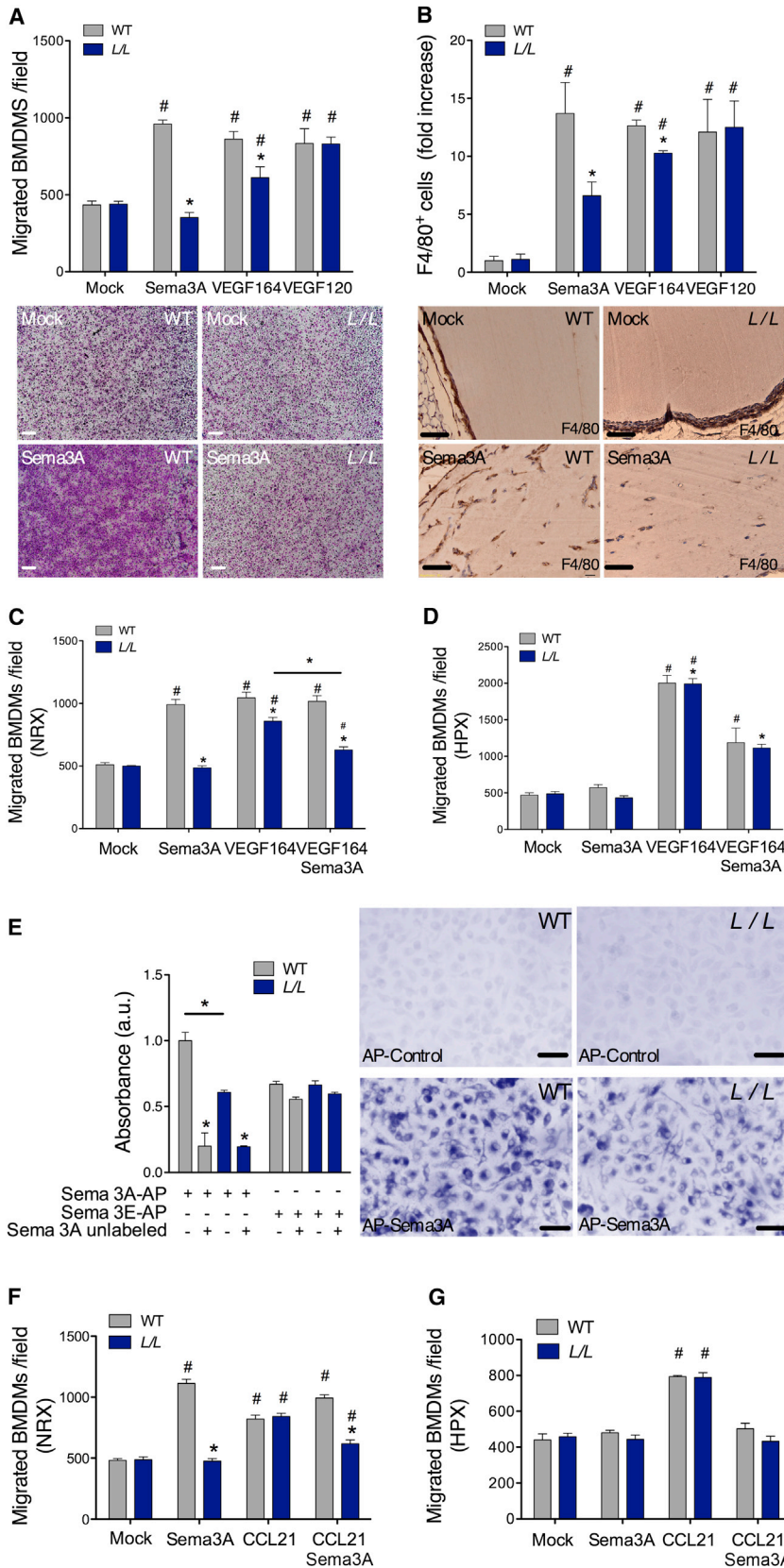


Figure 6. Sema3A Attracts or Retains Macrophages Depending on the Presence or Absence of Nrp1

(A) Migration of WT and *Nrp1*-KO (*L/L*) BMDMs toward Sema3A, VEGF₁₆₄, or VEGF₁₂₀.

(B) Migration of F4/80⁺ macrophages in subcutaneous matrigel plugs supplemented with Sema3A, VEGF₁₆₄, or VEGF₁₂₀.

(C and D) Migration of WT and *Nrp1*-KO (*L/L*) BMDMs toward Sema3A and VEGF₁₆₄, alone or in combination, under normoxic (NRX; C) or hypoxic (HPX; D) conditions.

(E) Binding of Sema3A-AP (or Sema3E-AP as control) to WT and *Nrp1*-KO (*L/L*) BMDMs in absence or presence of 2-fold molar excess of unlabeled Sema3A. Cell-bound AP activity was revealed in situ using colorimetric reactions as shows in micrographs.

(F and G) Migration of WT and *Nrp1*-KO (*L/L*) BMDMs toward Sema3A and VEGF₁₆₄, alone or in combination, under normoxic (NRX; F) or hypoxic (HPX; G) conditions.

**p* < 0.05 versus WT; #*p* < 0.05 versus mock. Scale bars: 100 μm in (A), 50 μm in (B), and 20 μm in (E). All graphs show mean ± SEM of four independent experiments. See also Figure S4.

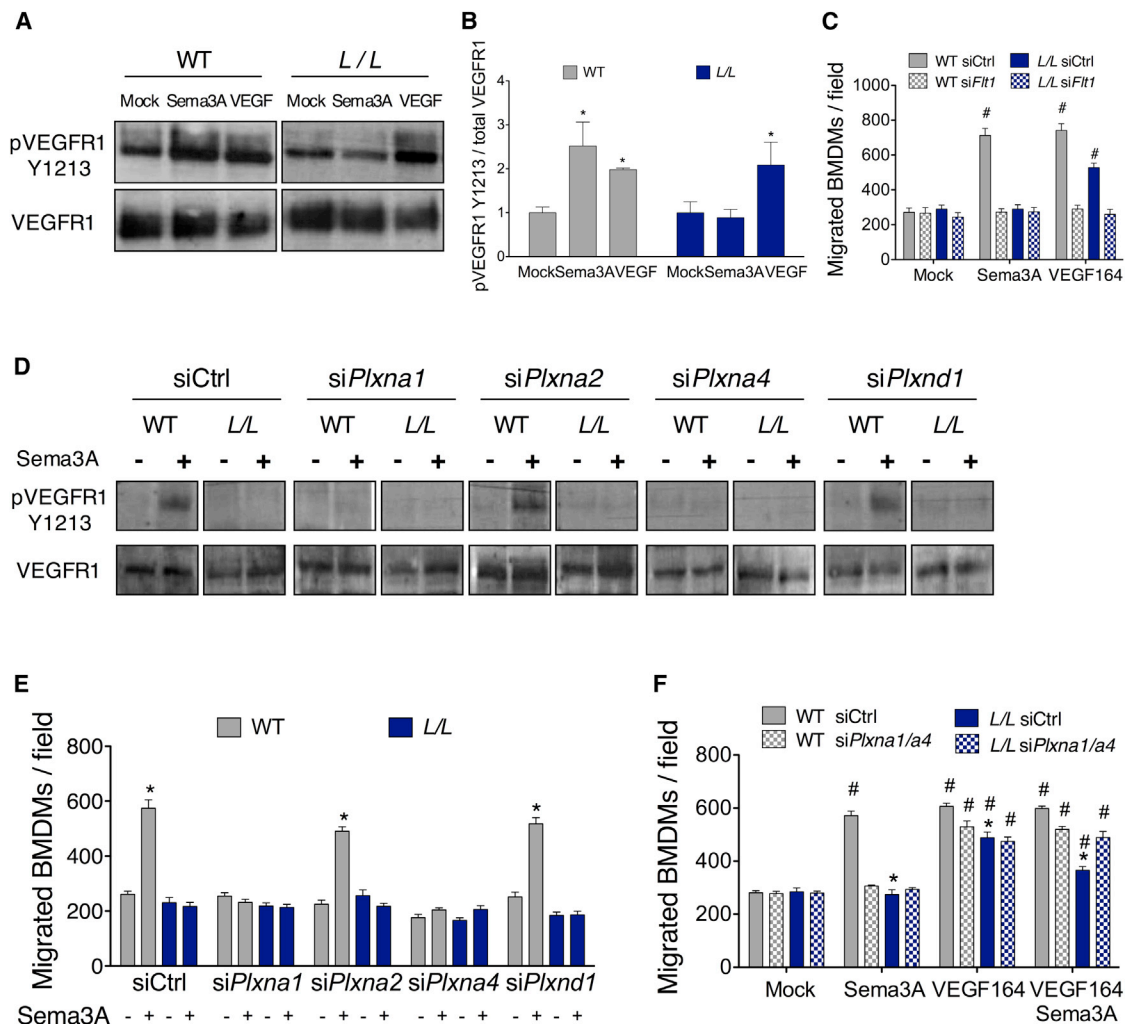


Figure 7. TAM Attraction by Semaphorins Involves VEGFR1, whereas Their Retention Requires PlexinA1/A4 Only

(A and B) Western blot (A) and densitometry (B) for VEGFR1 Y1213 phosphorylation in WT and *Nrp1*-KO (*L/L*) BMDMs upon Semaphorin 3A and VEGF stimulation. (C) Migration toward Semaphorin 3A or VEGF₁₆₄ of WT and *Nrp1*-KO (*L/L*) BMDMs silenced for *Flt1* (si*Flt1*) or scramble control (shCtrl). (D and E) VEGFR1 phosphorylation (D) and migration (E) in Semaphorin 3A-treated WT and *Nrp1*-KO (*L/L*) BMDMs, upon silencing of *Plxna1*, *Plxna2*, *Plxna4*, or *Plxnd1*. (F) Migration of WT and *Nrp1*-KO (*L/L*) BMDMs toward Semaphorin 3A and VEGF₁₆₄, alone or together, upon combined silencing of *Plxna1* and *Plxna4*. **p* < 0.05 versus WT; #*p* < 0.05 versus mock. All graphs show mean ± SEM of three to four independent experiments. See also Figure S5.

detectable (Figures 6F and 6G). These data further support the conclusion that, while Semaphorin 3A attracts macrophages in a *Nrp1*-dependent manner, it is still active and can convey a migration-inhibitory effect upon *Nrp1* downregulation in the same cells.

Semaphorin 3A Activates Opposite Signaling in Presence or Absence of *Nrp1*

Semaphorins are mainly known as repelling signals, acting through receptors called plexins. However, when plexins transactivate receptor tyrosine kinases (RTKs), semaphorin signals can be converted into attractive cues (Tamagnone, 2012). At least in one case, this was found to implicate the expression of *Nrp1* (Bellon et al., 2010). While studying Semaphorin 3A-mediated activation of RTKs in macrophages, we found that Semaphorin 3A induced VEGFR1 Tyr1213 phosphorylation more potently than

VEGF₁₆₄ itself. Loss of *Nrp1* in macrophages completely abrogated Semaphorin 3A-dependent VEGFR1 activation without significantly affecting the response to VEGF (Figures 7A and 7B).

We then knocked down VEGFR1 in both WT and *Nrp1*-KO BMDMs (Figure S5A) and assessed the biological consequences on Semaphorin 3A-mediated migration. Whereas *Nrp1* was largely dispensable for the migratory response toward VEGF₁₆₄, the knockdown of VEGFR1 entirely prevented the migration of both WT and *Nrp1*-KO macrophages in response to either Semaphorin 3A or VEGF₁₆₄. This suggested that *Nrp1* requires VEGFR1 to transduce Semaphorin 3A-mediated attractive signals, whereas VEGFR1 alone can mediate VEGF activity in macrophages (Figure 7C).

We then evaluated the expression of plexins known to form semaphorin holoreceptors in association with *Nrp1*, namely PlexinA1, PlexinA2, PlexinA3, PlexinA4, and PlexinD1 (Tamagnone, 2012). All these plexins, except PlexinA3, were detectable

in TAMs and BMDMs and equally expressed in both WT and *Nrp1*-KO cells (Figures S5B and S5C). Silencing of PlexinA1 or PlexinA4 (but not of PlexinA2 or PlexinD1) in WT BMDMs (Figure S5D) abrogated *Sema3A*-mediated VEGFR1 phosphorylation and migration as potently as genetic deletion of *Nrp1* (Figures 7D and 7E). These cells were still migrating in response to serum stimulation, confirming their viability (Figures S5E and S5F).

Moreover, upon costimulation with *Sema3A* and VEGF, silencing of PlexinA1 and PlexinA4 prevented the migratory blockade orchestrated by *Sema3A* in *Nrp1*-KO BMDMs (Figure 7F). Thus, in presence of *Nrp1*, a *Sema3A*/PlexinA1/PlexinA4 axis mediates attractive cues via VEGFR1 transactivation, which are reverted into stop signals in the absence of *Nrp1*.

Sema3A Defines TAM Positioning within the Tumor

To assess the specific role of *Sema3A* in vivo, we used two complementary strategies. First, we used *Nrp1*^{Sema-} knock-in (KI) mice, which have a disrupted *Sema3A*-*Nrp1* binding site that leaves VEGF₁₆₅-*Nrp1* binding unaffected (Gu et al., 2003). As expected, *Nrp1*^{Sema-} macrophages did not migrate toward *Sema3A* whereas they responded normally to either VEGF₁₆₄ or VEGF₁₂₀ (Figure 8A). Compared to control mice (WT → WT), WT recipient mice transplanted with bone marrow (BM) cells from *Nrp1*^{Sema-} mice (KI → WT) displayed tumor growth inhibition and decreased vessel area and density, accompanied by increased tumor hypoxia and macrophage infiltration (Figures 8B–8G). Importantly, *Nrp1*^{Sema-} TAMs failed to enter hypoxic tumor regions, thus resembling the overall phenotype observed in tumor-bearing *LysM-Cre;Nrp1*^{L/L} mice (Figure 8H).

Second, we established subcutaneous tumors by injection of *Sema3A*-silenced LLC (LLC-Sh3A) or scrambled controls (LLC-ShCtrl) in WT and *LysM-Cre;Nrp1*^{L/L} mice. *Sema3a* knockdown was 85% in normoxia and completely prevented hypoxic induction of *Sema3a* (Figure S6A). In vitro proliferation of LLC-Sh3A and LLC-ShCtrl was comparable (Figure S6B). However, LLC-Sh3A tumors in WT mice displayed growth and vessel inhibition, as well as TAM exclusion from hypoxic areas, to a similar extent as LLC-ShCtrl tumors in *LysM-Cre;Nrp1*^{L/L} mice. Yet, *Sema3A* silencing did not further affect these parameters in *LysM-Cre;Nrp1*^{L/L} mice (Figures 8I–8N). All these data indicate that cancer cell-derived *Sema3A*, not VEGF, is responsible for TAM entry into hypoxic niches through *Nrp1* signaling.

DISCUSSION

Several hypotheses have proposed how TAMs might be recruited to and retained in the hypoxic tumor microenvironment, including hypoxia-mediated upregulation of chemoattractants and downregulation of chemokine receptors (Murdoch and Lewis, 2005). We describe a mechanism whereby *Nrp1* in macrophages is dispensable for their recruitment from the bloodstream but necessary for TAM positioning in hypoxic niches. Because macrophages differentiate from extravasated circulating monocytes, TAMs will initially accumulate in the proximity of the vascularized and perfused niche. From there, they will then move toward avascular/hypoxic areas of the tumor where they presumably clear necrotic cell debris. We now show that hypoxia upregulates *Sema3A* and VEGF, and these signals act as macro-

phage attractants by inducing, respectively, *Nrp1*-dependent or *Nrp1*-independent VEGFR1 transactivation (Figure 8O). Once macrophages localize in the hypoxic area, *Nrp1* expression in TAMs is downregulated terminating their migratory response to *Sema3A*, and therefore they remain entrapped on site. Notably, TAMs expressing a *Nrp1* mutant that cannot bind *Sema3A* (but that still retains its ability to bind VEGF) fail to enter the hypoxic regions of the tumor similarly to *Nrp1*-KO TAMs. These data indicate that VEGF signaling is not sufficient to drive TAM localization into hypoxic areas and support the idea of the presence of inhibitory signals able to blunt TAM attraction by VEGF and other factors (such as CCL21). We found that *Sema3A* itself can play such a role upon downregulation of *Nrp1* expression in TAMs by mediating plexin-dependent stop signals. Further work will define if the mechanism proposed by our study holds true in other pathologies. For instance, *Nrp1* in macrophages is not required for developmental angiogenesis (not shown and Fantin et al., 2013), likely because the expression of its ligand *Sema3A* starts later during embryogenesis (Püschel et al., 1995).

Whereas *Nrp1* has been considered a major component of the *Sema3A* receptor complex in association with plexins, we report an *Nrp1*-independent specific binding of *Sema3A* to macrophages, deploying inhibition of chemotactic signaling via PlexinA1/A4 effectors. X-ray crystallographic analyses demonstrated that *Sema3A* carries the same structural features enabling other semaphorins to directly interact with plexins and trigger their inhibitory signals (Janssen et al., 2012; Nogi et al., 2010). However, this association seems to require the stabilizer function of additional ligand-binding components, commonly identified in *Nrp1*. In the absence of *Nrp1*, *Sema3A* binding is reduced but not abrogated, consistent with our observations in macrophages. Previous reports illustrated the interaction between *Sema3A* and chondroitin-sulfate glycosaminoglycans on the plasma membrane (De Wit et al., 2005). The punctate distribution of these molecules at the cell surface is indeed reminiscent of that observed for *Sema3A* bound to neuronal cells (De Wit et al., 2005) and, in our study, to macrophages. This may suggest a role for proteoglycans in *Sema3A* receptor complexes found in macrophages, in association with plexins, similar to what is known for other cell guidance cues and soluble factors (de Wit and Verhaagen, 2007; Fuster and Esko, 2005).

TAMs in avascular/hypoxic areas represent a deadly combination because TAMs respond to hypoxia with an altered gene expression profile leading to the development of a distinct protumoral phenotype that favors angiogenesis, metastasis, and suppresses antitumor immune responses (Burke et al., 2003; Doedens et al., 2010; Movahedi et al., 2010). Here, we formally prove that accumulation of TAMs in normoxic regions and their exclusion from hypoxic tumor regions (upon loss of *Nrp1*) blunt their angiogenic and immunosuppressive capacity, resulting in reduced vessel branching and Th1/CTL-mediated antitumor immune responses. The release of cytokines, such as interferon gamma (IFN γ), by Th1 T cells and especially by CTL will polarize the newly recruited TAMs in M1-like cytotoxic macrophages, thus initiating a feed-forward loop that enhances antitumor immunity (Biswas and Mantovani, 2010; Coussens et al., 2013; Johansson et al., 2008). Reduced angiogenesis and tumor perfusion will also initiate a feed-forward loop because the resulting hypoxia will lead to more TAM recruitment (Eltzschig and

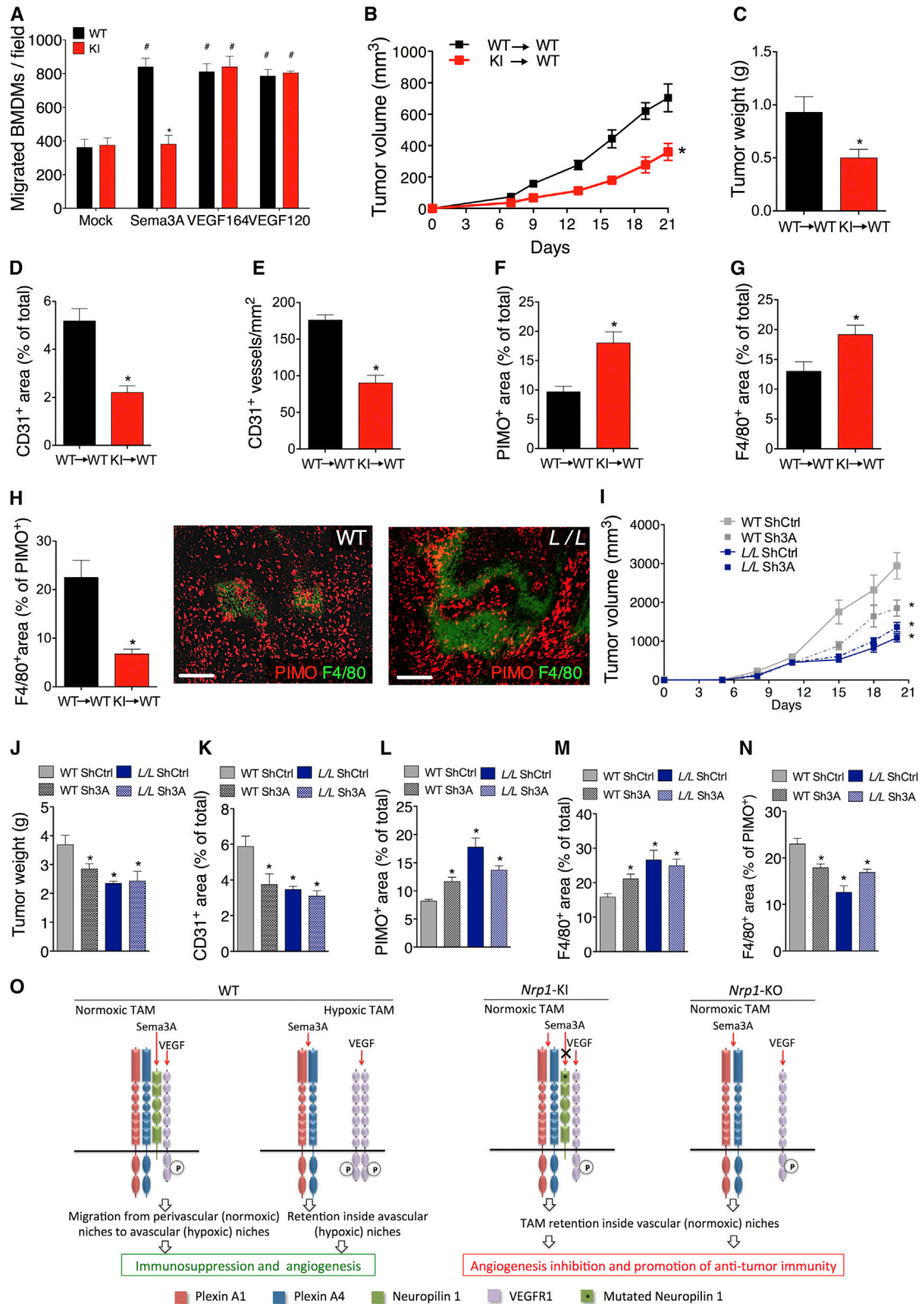


Figure 8. Sema3A Defines TAM Positioning within the Tumor

(A) Migration of WT and *Nrp1*^{Sema3A}- (KI) BMDMs in response to Sema3A, VEGF₁₆₄, or VEGF₁₂₀.

(B and C) Growth (B) and weight (C) of subcutaneous LLC tumors injected in mice transplanted with BM from WT or *Nrp1*^{Sema3A}- mice (WT→WT and KI→WT, respectively).

(legend continued on next page)

Carmeliet, 2011; Murdoch and Lewis, 2005). Nevertheless, these TAMs will not enter the hypoxic niches because of lack of Nrp1, and this will perpetuate their antitumor phenotype. These findings might explain some observations in human tumor biopsies where higher numbers of TAMs do not always correlate with a worse prognosis but rather with a favorable disease outcome or the clinical correlation between different TAM localizations and patient survival (De Palma and Lewis, 2013).

Different from what occurs in macrophages, Sema3A-mediated Nrp1 signaling acts as a restrictive signal for EC migration (Serini et al., 2003) and exogenous delivery of Sema3A in tumor models can inhibit angiogenesis and hinder tumor growth (Casazza et al., 2011; Maione et al., 2009, 2012). Notably, in these previous studies, TAM distribution into tumors had not been tested. Moreover, while guidance cues such as Sema3A are known to organize cell migration and neurite extension in a topographically controlled manner, their exogenous delivery into tissues may elicit pharmacological effects overwhelming the functional complexity of the endogenous signals. Indeed, the formation of a vascular network is a dynamic process that depends on pro-angiogenic and anti-angiogenic stimuli (Mazzone et al., 2009). Once recruited to the tumor from the bloodstream, TAMs will be attracted from perivascular/normoxic into avascular/hypoxic niches by Sema3A via an Nrp1/PlexinA1/A4/VEGFR1 signaling platform. Downregulation of Nrp1 arrests TAMs in their position through Nrp1-independent Sema3A-mediated PlexinA1/A4 signals. Here, TAMs secrete “angiokines” such as VEGF and Sema3A, and matrix metalloproteases including MMP2 and MMP9 (Movahedi et al., 2010; Murdoch and Lewis, 2005; Pucci et al., 2009). ECs will thus follow the macrophages into the hypoxic regions of the tumor, where they are attracted by VEGF, but their migration will be partly limited by Sema3A-repelling signals, as Nrp1 expression in ECs is induced by hypoxia, in contrast to macrophages (Ottino et al., 2004; Zhang et al., 2001). Future studies will elucidate how *Nrp1* is inversely regulated by hypoxia in different cellular contexts. The reported ability of Sema3A-Nrp1 signaling to guide TAM migration into hypoxic niches, where they eventually are entrapped, is reminiscent of the activity of axonal guidance cues featuring navigation “go” and “stop” signals at distinctive sites, depending on the level of signaling components (Guthrie, 1999; Nawabi et al., 2010; Schwarz and Ruhrberg, 2010). To prove the functional relevance of this specific mechanism in vivo, we selectively inhibited Sema3A binding to Nrp1 in macrophages or we silenced Sema3A in cancer cells, and found that, consistent with preventing TAM migration into hypoxic niches, this reduced

angiogenesis and tumor growth. Overall, our results and the previous works show that localized activity of endogenous Sema3A in individual cell populations versus pharmacological administration of exogenous Sema3A can have divergent effects on tumor growth in vivo. Interestingly, antibodies selectively blocking Sema3A binding to Nrp1, despite their scarce activity on ECs in vitro, inhibit angiogenesis and vessel remodeling in vivo with a similar efficacy as antibodies blocking VEGF binding to Nrp1, thus possibly implying the effective blockade of other pro-angiogenic cells such as macrophages (Pan et al., 2007).

Consistent with the finding that Sema3A can mediate attractive or repulsive cues, its expression has been associated with both tumor progression (Biankin et al., 2012; Müller et al., 2007) and tumor suppression (Maione et al., 2009; Yacoub et al., 2009); however the functional relevance of the endogenous molecule in adult tissues has not been fully elucidated. Our study sheds light on the role of Sema3A/Nrp1 signaling in the guidance of macrophages into hypoxic niches. Thus, Sema3A expression in tumors may also predict the ability to drive TAMs toward hypoxic niches to escape antitumor immunity and to promote vascularization.

EXPERIMENTAL PROCEDURES

More detailed methods can be found in the [Supplemental Experimental Procedures](#).

Tumor Models

LLC cells were injected subcutaneously (2×10^6 cells) or orthotopically (1×10^6 cells); Panc02 was injected into the tail of the pancreas (1 ± 10^6 cells). PyMT tumors were classified as before (Lin et al., 2003). All mouse procedures were approved by the Institutional Animal Care and Research Advisory Committee of the K.U. Leuven.

BM Transplantation

Lethally irradiated C56BL/6 mice (9.5 Gy) were intravenously injected with 10^7 BM cells from *Nrp1*^{Sema3A} mice. Tumor experiments were initiated 6 weeks after BM reconstitution.

Western Blot and Immunohistochemistry

Protein extraction was performed using extraction buffer (20 mM Tris HCl, 150 mM NaCl, 1% Triton X-100, 10% glycerol, and 5 mM EDTA). Immunostaining protocols and hypoxia detection were performed as before (Mazzone et al., 2009). Tumor perfusion was assessed with intravenous injection of 0.05 mg lectin-FITC.

FACS Analysis and Flow Sorting of Tumor-Associated Cells

LLC subcutaneous tumors were minced in RPMI medium containing 0.1% collagenase type I and 0.2% dispase type I (30 min at 37°C), passed through

(D–F) Tumor vessel area (D), tumor vessel density (E), and tumor hypoxia (F) in WT → WT and KI → WT mice.

(G) Histological quantification of F4/80⁺ TAM accumulation in WT → WT and KI → WT mice.

(H) Quantification and micrographs showing F4/80⁺ TAMs in PIMO⁺ hypoxic tumor regions.

(I–N) Growth (I), weight (J), CD31⁺ vessel area (K), PIMO⁺ hypoxic area (L), total F480⁺ TAM accumulation (M), and hypoxic TAM accumulation (N) in tumors derived from Sema3A-silenced LLC (Sh3A) or from scramble control LLC (ShCtrl), injected subcutaneously in WT and LysM-Cre;*Nrp1*^{L/L} (L/L) mice.

(O) VEGF and Sema3A attract TAMs from peri-vascular (normoxic) areas to avascular (hypoxic) niches through VEGFR1 transactivation. While VEGF works independently of Nrp1, Sema3A-mediated VEGFR1 activation requires Nrp1 as well as PlexinA1 and PlexinA4. Upon repression of Nrp1 by hypoxia, Sema3A retains TAMs inside the hypoxic niche through PlexinA1/A4 signaling. Hypoxic TAMs acquire an immunosuppressive and pro-angiogenic phenotype, which contributes to tumor growth and metastasis. Because of loss of Sema3A binding to Nrp1 in *Nrp1*^{Sema3A} (KI) TAMs or gene deletion in *Nrp1*-KO TAMs, Sema3A does not attract but rather entraps TAMs in the perivascular (normoxic) areas countering attraction by VEGF or other cytokines in a PlexinA1/A4-dependent manner. Normoxic TAMs are then less angiogenic and more antitumoral.

n = 4 in (A), n = 10 in (B–H), and n = 6–8 in (I–N). *p < 0.05 versus WT; #p < 0.05 versus mock. Scale bars: 100 μm. All graphs show mean ± SEM. See also [Figure S6](#).

a 19 G needle, and filtered. After RBC lysis, cells were resuspended in fluorescence-activated cell sorting buffer (PBS containing 2% fetal bovine serum and 2 mM EDTA) and incubated with Mouse BD Fc Block purified antimouse CD16/CD32 mAb (BD PharMingen), followed by staining with anti-F4/80, CD3, CD4, CD8, CD115, Ly6C, Ly6G, CD11c, CD11b, and MRC1 for 20 min at 4°C. F4/80⁺ TAMs were sorted from subcutaneous LLC tumors; hypoxic TAMs were sorted as before (Movahedi et al., 2010).

Migration Assays

Six-week-old mice were subcutaneously injected with 500 μ l of growth factor-reduced Matrigel (BD Biosciences), supplemented with either PBS or with 1 μ g purified murine Sema3A, VEGF₁₆₄, or VEGF₁₂₀ (R&D). After 5 days, mice were sacrificed and macrophage recruitment was evaluated by histological analysis. Skin inflammation was induced by ear painting with the phorbol ester TPA and analyzed after 24 hr.

Endothelial Cell Capillary Formation

Sorted TAMs or 10⁵ BMDMs were embedded in growth factor-reduced Matrigel (BD Biosciences). After 36 hr, 10⁴ human umbilical vein endothelial cells (HUVECs) fluorescently labeled with PKH-26 (Sigma-Aldrich) were added to the Matrigel. Alternatively, a conditioned medium (obtained from 2.5 \times 10⁵ BMDMs or sorted TAMs in culture for 36 hr) was used to resuspend 10⁴ HUVECs, which were then seeded directly on Matrigel. After 4 hr, capillary formation was analyzed by measuring the number of branches and length of the vascular network using ImageJ software.

Macrophage Cytotoxicity Assay

LLC cells were labeled with 1 μ Ci/ml ³H-Thymidine for 20 hr. Then, 10⁴ cells were seeded together with increasing concentrations of activated BMDMs (20 ng/ml IFN γ + 100 ng/ml lipopolysaccharide for 24 hr) or sorted TAMs. After 24 hr, LLC cell death was detected by measuring radioactivity in a cell-free medium.

T Cell Suppression

For T cell suppression, 2 \times 10⁵ naive C57BL/6 splenocytes were added to increasing concentrations of BMDMs or sorted TAMs, and stimulated with 1 μ g/ml anti-CD3. After 24 hr, cells were pulsed with ³H-thymidine (PerkinElmer) and incubated for another 18 hr before incorporated radioactivity was measured.

T Cell Depletion

Th-cell and CTL depletion was performed in LLC tumor-bearing mice with intraperitoneal injection of 0.2 mg anti-CD4 (GK1.5) or anti-CD8 (53-6.7; BioXCell), respectively, or rat IgG isotypes as control, every third day, starting the sixth day after tumor injection.

Statistics

Data indicate mean \pm SEM of representative experiments. Statistical significance was calculated by two-tailed unpaired t test for two data sets (or Chi-square for PyMT tumor staging and Gehan-Breslow-Wilcoxon for the survival upon orthotopic LLC tumor implantation), with $p < 0.05$ considered as statistically significant.

SUPPLEMENTAL INFORMATION

Supplemental Information includes Supplemental Experimental Procedures, six figures, and one table and can be found with this article online at <http://dx.doi.org/10.1016/j.ccr.2013.11.007>.

ACKNOWLEDGMENTS

The authors thank J. Serneels, Y. Jonsson, and Y. Elkrim for technical assistance and Dr. Serini, Dr. Carmeliet, and Dr. De Palma for comments. M.M. was supported by an ERC starting grant, L.T. by AIRC-IG no.11-598 and MIUR-PRIN grants, A.C. by EMBO, and D.L. by VLK. *Nrp1^{L/L}* and *Nrp1^{Sema}* mice were a gift of Dr. Gu (Harvard University) and Dr. Ginty (Johns Hopkins); the iCSF1R-Cre line was provided by Dr. Pollard (Albert Einstein College of Medicine).

Received: February 13, 2013

Revised: October 4, 2013

Accepted: November 10, 2013

Published: December 9, 2013

REFERENCES

- Bellon, A., Luchino, J., Haigh, K., Rougon, G., Haigh, J., Chauvet, S., and Mann, F. (2010). VEGFR2 (KDR/Flk1) signaling mediates axon growth in response to semaphorin 3E in the developing brain. *Neuron* 66, 205–219.
- Biankin, A.V., Waddell, N., Kassahn, K.S., Gingras, M.C., Muthuswamy, L.B., Johns, A.L., Miller, D.K., Wilson, P.J., Patch, A.M., Wu, J., et al.; Australian Pancreatic Cancer Genome Initiative (2012). Pancreatic cancer genomes reveal aberrations in axon guidance pathway genes. *Nature* 491, 399–405.
- Biswas, S.K., and Mantovani, A. (2010). Macrophage plasticity and interaction with lymphocyte subsets: cancer as a paradigm. *Nat. Immunol.* 11, 889–896.
- Blouw, B., Song, H., Tihan, T., Bosze, J., Ferrara, N., Gerber, H.P., Johnson, R.S., and Bergers, G. (2003). The hypoxic response of tumors is dependent on their microenvironment. *Cancer Cell* 4, 133–146.
- Bruder, D., Probst-Kepper, M., Westendorf, A.M., Geffers, R., Beissert, S., Loser, K., von Boehmer, H., Buer, J., and Hansen, W. (2004). Neuropilin-1: a surface marker of regulatory T cells. *Eur. J. Immunol.* 34, 623–630.
- Burke, B., Giannoudis, A., Corke, K.P., Gill, D., Wells, M., Ziegler-Heitbrock, L., and Lewis, C.E. (2003). Hypoxia-induced gene expression in human macrophages: implications for ischemic tissues and hypoxia-regulated gene therapy. *Am. J. Pathol.* 163, 1233–1243.
- Casazza, A., Fu, X., Johansson, I., Capparuccia, L., Andersson, F., Giustacchini, A., Squadrito, M.L., Venneri, M.A., Mazzone, M., Larsson, E., et al. (2011). Systemic and targeted delivery of semaphorin 3A inhibits tumor angiogenesis and progression in mouse tumor models. *Arterioscler. Thromb. Vasc. Biol.* 31, 741–749.
- Catalano, A. (2010). The neuroimmune semaphorin-3A reduces inflammation and progression of experimental autoimmune arthritis. *J. Immunol.* 185, 6373–6383.
- Catalano, A., Caprari, P., Moretti, S., Faronato, M., Tamagnone, L., and Procopio, A. (2006). Semaphorin-3A is expressed by tumor cells and alters T-cell signal transduction and function. *Blood* 107, 3321–3329.
- Coussens, L.M., Zitvogel, L., and Palucka, A.K. (2013). Neutralizing tumor-promoting chronic inflammation: a magic bullet? *Science* 339, 286–291.
- De Palma, M., and Lewis, C.E. (2013). Macrophage regulation of tumor responses to anticancer therapies. *Cancer Cell* 23, 277–286.
- de Wit, J., and Verhaagen, J. (2007). Proteoglycans as modulators of axon guidance cue function. *Adv. Exp. Med. Biol.* 600, 73–89.
- De Wit, J., De Winter, F., Klooster, J., and Verhaagen, J. (2005). Semaphorin 3A displays a punctate distribution on the surface of neuronal cells and interacts with proteoglycans in the extracellular matrix. *Mol. Cell. Neurosci.* 29, 40–55.
- Delgoffe, G.M., Woo, S.R., Turnis, M.E., Gravano, D.M., Guy, C., Overacre, A.E., Bettini, M.L., Vogel, P., Finkelstein, D., Bonnevier, J., et al. (2013). Stability and function of regulatory T cells is maintained by a neuropilin-1-semaphorin-4a axis. *Nature* 501, 252–256.
- Doedens, A.L., Stockmann, C., Rubinstein, M.P., Liao, D., Zhang, N., DeNardo, D.G., Coussens, L.M., Karin, M., Goldrath, A.W., and Johnson, R.S. (2010). Macrophage expression of hypoxia-inducible factor-1 alpha suppresses T-cell function and promotes tumor progression. *Cancer Res.* 70, 7465–7475.
- Eltzschig, H.K., and Carmeliet, P. (2011). Hypoxia and inflammation. *N. Engl. J. Med.* 364, 656–665.
- Fantini, A., Vieira, J.M., Gestri, G., Denti, L., Schwarz, Q., Prykhodzij, S., Peri, F., Wilson, S.W., and Ruhrberg, C. (2010). Tissue macrophages act as cellular chaperones for vascular anastomosis downstream of VEGF-mediated endothelial tip cell induction. *Blood* 116, 829–840.
- Fantini, A., Vieira, J.M., Plein, A., Denti, L., Fruttiger, M., Pollard, J.W., and Ruhrberg, C. (2013). NRP1 acts cell autonomously in endothelium to promote tip cell function during sprouting angiogenesis. *Blood* 121, 2352–2362.

- Fuster, M.M., and Esko, J.D. (2005). The sweet and sour of cancer: glycans as novel therapeutic targets. *Nat. Rev. Cancer* 5, 526–542.
- Gerhardt, H., Ruhrberg, C., Abramsson, A., Fujisawa, H., Shima, D., and Betsholtz, C. (2004). Neuropilin-1 is required for endothelial tip cell guidance in the developing central nervous system. *Dev. Dyn.* 231, 503–509.
- Gu, C., Rodriguez, E.R., Reimert, D.V., Shu, T., Fritzsche, B., Richards, L.J., Kolodkin, A.L., and Ginty, D.D. (2003). Neuropilin-1 conveys semaphorin and VEGF signaling during neural and cardiovascular development. *Dev. Cell* 5, 45–57.
- Guthrie, S. (1999). Axon guidance: starting and stopping with slit. *Curr. Biol.* 9, R432–R435.
- Hansen, W., Hutzler, M., Abel, S., Alter, C., Stockmann, C., Kliche, S., Albert, J., Sparwasser, T., Sakaguchi, S., Westendorf, A.M., et al. (2012). Neuropilin 1 deficiency on CD4⁺Foxp3⁺ regulatory T cells impairs mouse melanoma growth. *J. Exp. Med.* 209, 2001–2016.
- Hayashi, M., Nakashima, T., Taniguchi, M., Kodama, T., Kumanogoh, A., and Takayanagi, H. (2012). Osteoprotection by semaphorin 3A. *Nature* 485, 69–74.
- Hong, T.M., Chen, Y.L., Wu, Y.Y., Yuan, A., Chao, Y.C., Chung, Y.C., Wu, M.H., Yang, S.C., Pan, S.H., Shih, J.Y., et al. (2007). Targeting neuropilin 1 as an anti-tumor strategy in lung cancer. *Clin. Cancer Res.* 13, 4759–4768.
- Janssen, B.J., Malinauskas, T., Weir, G.A., Cader, M.Z., Siebold, C., and Jones, E.Y. (2012). Neuropilins lock secreted semaphorins onto plexins in a ternary signaling complex. *Nat. Struct. Mol. Biol.* 19, 1293–1299.
- Johansson, M., Denardo, D.G., and Coussens, L.M. (2008). Polarized immune responses differentially regulate cancer development. *Immunol. Rev.* 222, 145–154.
- Kolodkin, A.L., Levengood, D.V., Rowe, E.G., Tai, Y.T., Giger, R.J., and Ginty, D.D. (1997). Neuropilin is a semaphorin III receptor. *Cell* 90, 753–762.
- Liang, W.C., Dennis, M.S., Stawicki, S., Chantry, Y., Pan, Q., Chen, Y., Eigenbrot, C., Yin, J., Koch, A.W., Wu, X., et al. (2007). Function blocking antibodies to neuropilin-1 generated from a designed human synthetic antibody phage library. *J. Mol. Biol.* 366, 815–829.
- Lin, E.Y., Jones, J.G., Li, P., Zhu, L., Whitney, K.D., Muller, W.J., and Pollard, J.W. (2003). Progression to malignancy in the polyoma middle T oncoprotein mouse breast cancer model provides a reliable model for human diseases. *Am. J. Pathol.* 163, 2113–2126.
- Maione, F., Molla, F., Meda, C., Latini, R., Zentilin, L., Giacca, M., Seano, G., Serini, G., Bussolino, F., and Giraudo, E. (2009). Semaphorin 3A is an endogenous angiogenesis inhibitor that blocks tumor growth and normalizes tumor vasculature in transgenic mouse models. *J. Clin. Invest.* 119, 3356–3372.
- Maione, F., Capano, S., Regano, D., Zentilin, L., Giacca, M., Casanovas, O., Bussolino, F., Serini, G., and Giraudo, E. (2012). Semaphorin 3A overcomes cancer hypoxia and metastatic dissemination induced by antiangiogenic treatment in mice. *J. Clin. Invest.* 122, 1832–1848.
- Mazzone, M., Dettori, D., Leite de Oliveira, R., Loges, S., Schmidt, T., Jonckx, B., Tian, Y.M., Lanahan, A.A., Pollard, P., Ruiz de Almodovar, C., et al. (2009). Heterozygous deficiency of PHD2 restores tumor oxygenation and inhibits metastasis via endothelial normalization. *Cell* 136, 839–851.
- Movahedi, K., Laoui, D., Gysemans, C., Baeten, M., Stangé, G., Van den Bossche, J., Mack, M., Pipeleers, D., In't Veld, P., De Baetselier, P., and Van Ginderachter, J.A. (2010). Different tumor microenvironments contain functionally distinct subsets of macrophages derived from Ly6C(high) monocytes. *Cancer Res.* 70, 5728–5739.
- Müller, M.W., Giese, N.A., Swiercz, J.M., Ceyhan, G.O., Esposito, I., Hinz, U., Büchler, P., Giese, T., Büchler, M.W., Offermanns, S., and Friess, H. (2007). Association of axon guidance factor semaphorin 3A with poor outcome in pancreatic cancer. *Int. J. Cancer* 121, 2421–2433.
- Murdoch, C., and Lewis, C.E. (2005). Macrophage migration and gene expression in response to tumor hypoxia. *Int. J. Cancer* 117, 701–708.
- Nawabi, H., Briançon-Marjollet, A., Clark, C., Sanyas, I., Takamatsu, H., Okuno, T., Kumanogoh, A., Bozon, M., Takeshima, K., Yoshida, Y., et al. (2010). A midline switch of receptor processing regulates commissural axon guidance in vertebrates. *Genes Dev.* 24, 396–410.
- Niedergethmann, M., Hildenbrand, R., Wostbrock, B., Hartel, M., Sturm, J.W., Richter, A., and Post, S. (2002). High expression of vascular endothelial growth factor predicts early recurrence and poor prognosis after curative resection for ductal adenocarcinoma of the pancreas. *Pancreas* 25, 122–129.
- Nogi, T., Yasui, N., Mihara, E., Matsunaga, Y., Noda, M., Yamashita, N., Toyofuku, T., Uchiyama, S., Goshima, Y., Kumanogoh, A., and Takagi, J. (2010). Structural basis for semaphorin signalling through the plexin receptor. *Nature* 467, 1123–1127.
- Ottino, P., Finley, J., Rojo, E., Otlecz, A., Lambrou, G.N., Bazan, H.E., and Bazan, N.G. (2004). Hypoxia activates matrix metalloproteinase expression and the VEGF system in monkey choroid-retinal endothelial cells: Involvement of cytosolic phospholipase A2 activity. *Mol. Vis.* 10, 341–350.
- Pan, Q., Chantry, Y., Liang, W.C., Stawicki, S., Mak, J., Rathore, N., Tong, R.K., Kowalski, J., Yee, S.F., Pacheco, G., et al. (2007). Blocking neuropilin-1 function has an additive effect with anti-VEGF to inhibit tumor growth. *Cancer Cell* 11, 53–67.
- Pucci, F., Venneri, M.A., Biziato, D., Nonis, A., Moi, D., Sica, A., Di Serio, C., Naldini, L., and De Palma, M. (2009). A distinguishing gene signature shared by tumor-infiltrating Tie2-expressing monocytes, blood “resident” monocytes, and embryonic macrophages suggests common functions and developmental relationships. *Blood* 114, 901–914.
- Püschel, A.W., Adams, R.H., and Betz, H. (1995). Murine semaphorin D/collapsin is a member of a diverse gene family and creates domains inhibitory for axonal extension. *Neuron* 14, 941–948.
- Qian, B.Z., Li, J., Zhang, H., Kitamura, T., Zhang, J., Campion, L.R., Kaiser, E.A., Snyder, L.A., and Pollard, J.W. (2011). CCL2 recruits inflammatory monocytes to facilitate breast-tumour metastasis. *Nature* 475, 222–225.
- Rolny, C., Mazzone, M., Tugues, S., Laoui, D., Johansson, I., Coulon, C., Squadrito, M.L., Segura, I., Li, X., Knevels, E., et al. (2011). HRG inhibits tumor growth and metastasis by inducing macrophage polarization and vessel normalization through downregulation of PlGF. *Cancer Cell* 19, 31–44.
- Schwarz, Q., and Ruhrberg, C. (2010). Neuropilin, you gotta let me know: should I stay or should I go? *Cell Adhes. Migr.* 4, 61–66.
- Serini, G., Valdembri, D., Zanivan, S., Morterra, G., Burkhardt, C., Caccavari, F., Zammataro, L., Primo, L., Tamagnone, L., Logan, M., et al. (2003). Class 3 semaphorins control vascular morphogenesis by inhibiting integrin function. *Nature* 424, 391–397.
- Soker, S., Takashima, S., Miao, H.Q., Neufeld, G., and Klagsbrun, M. (1998). Neuropilin-1 is expressed by endothelial and tumor cells as an isoform-specific receptor for vascular endothelial growth factor. *Cell* 92, 735–745.
- Takamatsu, H., Takegahara, N., Nakagawa, Y., Tomura, M., Taniguchi, M., Friedel, R.H., Rayburn, H., Tessier-Lavigne, M., Yoshida, Y., Okuno, T., et al. (2010). Semaphorins guide the entry of dendritic cells into the lymphatics by activating myosin II. *Nat. Immunol.* 11, 594–600.
- Takeda, Y., Costa, S., Delamarre, E., Roncal, C., Leite de Oliveira, R., Squadrito, M.L., Finisguerra, V., Deschoemaeker, S., Bruyère, F., Wenes, M., et al. (2011). Macrophage skewing by Phd2 haploinsufficiency prevents ischaemia by inducing arteriogenesis. *Nature* 479, 122–126.
- Tamagnone, L. (2012). Emerging role of semaphorins as major regulatory signals and potential therapeutic targets in cancer. *Cancer Cell* 22, 145–152.
- Tordjman, R., Lepelletier, Y., Lemarchandel, V., Cambot, M., Gaulard, P., Hermine, O., and Roméo, P.H. (2002). A neuronal receptor, neuropilin-1, is essential for the initiation of the primary immune response. *Nat. Immunol.* 3, 477–482.
- Yacoub, M., Coulon, A., Celhay, O., Irani, J., Cussenot, O., and Fromont, G. (2009). Differential expression of the semaphorin 3A pathway in prostatic cancer. *Histopathology* 55, 392–398.
- Zhang, Z.G., Tsang, W., Zhang, L., Powers, C., and Chopp, M. (2001). Up-regulation of neuropilin-1 in neovasculature after focal cerebral ischemia in the adult rat. *J. Cereb. Blood Flow Metab.* 21, 541–549.